EMITTANCE CONTROL IN THE PRESENCE OF COLLECTIVE EFFECTS IN THE FERMI@ELETTRA FREE ELECTRON LASER LINAC DRIVER*

S. Di Mitri#, E. Allaria, D. Castronovo, M. Cornacchia, W.M. Fawley, L. Fröhlich, E. Karantzoulis, G. Penco, C. Serpico, C. Spezzani, M. Trovo', M. Veronese, Elettra Trieste, Basovizza, Italy
L. Giannessi, ENEA, Frascati (Roma) & Elettra Trieste, Basovizza, Italy
P. Craievich, Elettra Trieste, Basovizza, Italy & PSI, Villigen, Switzerland
A.A. Lutman, Elettra Trieste, Basovizza, Italy & SLAC, Menlo Park, CA, USA
G. De Ninno, S. Spampinati, Elettra Trieste, Basovizza & University of Nova Gorica, Slovenia
M. Dal Forno, Elettra Trieste, Basovizza & University of Trieste, Trieste, Italy
E. Ferrari, Elettra Trieste, Basovizza & Università degli Studi di Trieste, Trieste, Italy

Abstract

Recent beam transport experiments conducted on the linac driving the FERMI@Elettra free electron laser (FEL) have provided new insights concerning the transverse emittance degradation due to both coherent synchrotron radiation (CSR) and geometric transverse wakefield (GTW), together with methods to counteract such degradation. For beam charges of several 100's of pC, optics control in a magnetic compressor helps to minimize the CSR effect by manipulating the H-function. We successfully extended this approach to the case of a modified double bend achromatic system, opening the door to relatively large bending angles and compact transfer lines. At the same time, the GTWs excited in few mm diameter iris collimators and accelerating structures have been characterized in terms of the induced emittance growth. A model integrating both CSR and GTW effects suggests that there is a limit on the maximum obtainable electron beam brightness in the presence of such collective effects.

INTRODUCTION TO FERMI FEL

FERMI@Elettra is a single-pass fourth generation light source user facility in operation at Elettra – Sincrotrone Trieste in Trieste, Italy [1, 2]. Table 1 shows the main electron and photon beam parameters.

Table 1: FERMI FEL Main Operational Parameters

Parameter	FEL-1	FEL-2	Unit
Charge	500	500	pC
Energy	0.9–1.2	1.0–1.5	GeV
Peak Current	600	400	A
Bunch Length, fw	0.7	1.0	ps
Norm. Emittance rms, slice	< 1.2	1.0	μm
Energy Spread rms, slice	< 250	< 250	keV
Fund. Wavelength	100 – 20	20 – 4	nm
Energy per pulse	< 400	< 100	μJ

*Work supported in part by the Italian Ministry of University and Research under grants FIRB-RBAP045JF2 and FIRB-RBAP06AWK3
#simone.dimitri@elettra.eu

An electron beam in the energy range 0.9–1.5 GeV drives two seeded FELs in the fundamental wavelength range 4–100 nm. The accelerator and FEL complex comprise the following parts: a photo-injector, and a main linac in which the beam is time-compressed in one or two-stages by a total factor of ~10; the transport system to the undulators; the undulator complex where the FEL radiation is generated; the photon beamlines, which transport the radiation from the undulator to the experimental area; and the experimental area itself.

IMPORTANCE OF PROJECTED TRANSVERSE EMITTANCE

Unlike linear colliders, where particle collisions effectively integrate over the entire bunch length, the FEL process takes place over short fractions of the electron bunch length. In fact, slice transverse emittance and slice energy spread may vary significantly along the bunch and thus give local regions where lasing may or may not occur. One could therefore argue that only *slice* electron beam quality is of interest, each slice typically being as long as the FEL slippage length. In this section we make the case that other considerations related to the electron beam control and optimization of the FEL performance justify an optimization of the four-dimensional electron beam normalized brightness, $B_{4D,n}$ that is defined as the final bunch peak current divided by the product of the transverse normalized *projected* emittances, *i.e.* integrated over the entire bunch length.

Electron –Photons Interaction in the Undulator

The need to control beam size and angular divergence along the undulator calls for measurements and manipulation of the electron beam optical parameters. The incoming electron beam optics must be matched to the design Twiss functions [3–5]. As a practical matter, optics matching is routinely performed by measuring the projected electron bunch transverse size [6, 7]. From an operational point of view, it is therefore important to ensure a projected emittance as close as possible to the slice one because this guarantees that most of the bunch slices are matched to the design optics; as a consequence, $B_{4D,n}$ is maximized.

ISBN 978-3-95450-126-7

Collective Effects in the Main Linac

As is well known, the horizontal (vertical) emittance is the area occupied by the particle ensemble in the x,x' (y,y') phase space, which is roughly the product of the transverse beam size and the transverse angular divergence. According to Liouville's theorem, its energy normalized value is a constant of motion during acceleration in absence of dissipative forces. In practice, the lower limit for the transverse emittance is set at the injector exit, where the space charge forces no longer act on the particles rearrangement in phase space. From this point on, at least two collective effects threaten to dilute the projected normalized emittance, namely CSR and GTW. We will show in the following that optics matching is one way to minimize them. As a consequence, control of the beam optical parameters is recommended not only in proximity of the undulator, as stated in the previous Section, but all along the accelerator.

FEL Spectrum

Even if slice parameters locally satisfied the FEL requirements, they would not ensure an efficient lasing, because the FEL intensity and its spectral properties may be degraded by (nonlinear) correlations between bunch's slices' coordinates. Such correlations translate into a projected emittance growth. This is the case, *e.g.*, of a bunch lasing in the presence of a pronounced distortion in the (z,x) or (z,y) physical space (so-called banana shape, when induced by GTW), which can either enlarge FEL bandwidth [8] or reduce FEL intensity [9], and a nonlinear energy chirp, which can affect both the FEL central wavelength of emission and its bandwidth [10, 11].

EMITTANCE GROWTH

In this article, we focus on the projected emittance growth along the FERMI linac driver induced by: CSR in the first magnetic chicane for bunch length compression and in the high energy transfer line (hereafter called Spreader) and by GTW in collimators and RF linac. Sources of emittance degradation and related strategies for emittance preservation are discussed below in the physical order the beam encounters them along the line. FERMI electron beam delivery system is sketched in Figure 1.

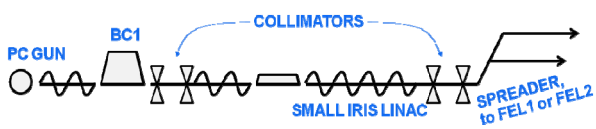

Figure 1: Sketch of FERMI FEL linac driver (not to scale).

CSR in Magnetic Compressor

A systematic characterization of the transverse emittance of a 200 pC, 6 ps long electron bunch has been performed in the FERMI@Elettra FEL first bunch compressor area [6]. This region includes a magnetic bunch length compressor, diagnostics and quadrupole magnets. At the time this experiment was done, the beam was time-compressed in one-stage, without linearization of the longitudinal phase space [12, 13]. Some growth of the normalized emittance was measured in the compressor area and compared to the estimate provided by the beam matrix formalism, by assuming that CSR mainly plays a role in the last dipole magnet of the four dipoles of a symmetric and achromatic chicane. We reformulate here that estimation in the extended form [14]:

$$\gamma\varepsilon \cong \gamma\varepsilon_0 \sqrt{1+\frac{H}{\varepsilon_0}\sigma^2_{\delta,CSR}}\,, \qquad (1)$$

where $\gamma\varepsilon_0$ is the unperturbed normalized horizontal emittance (γ is the relativistic Lorentz factor), $\sigma_{\delta,CSR}$ is the fractional energy spread induced by CSR [15] and $H=\left[\eta^2+(\beta\eta'+\alpha\eta)^2\right]/\beta$ is defined in terms of the Twiss functions and energy dispersion functions in the last dipole magnet. H-function reduces to the betatron function times the bending angle squared if the beam size is shrunk to a minimum, as shown in [6].

Control of the emittance growth was achieved by tuning the beam optics for each value of the compression factor, C. In particular, the horizontal betatron function was forced to the meter level in the second half of the chicane. At the end, the injector emittance was preserved for values of C up to 5, with a relative increment of only 3% and final normalized emittance smaller than 1.7 μm. This machine configuration has been adopted to optimize the FERMI FEL radiation output at wavelengths in the range 30–60 nm. Figure 2 shows the horizontal normalized emittance out of BC1, measured as function of C, which is varied by the upstream RF phase; BC1 is set at 85 mrad bending angle. The best achieved performance of the one-stage magnetic compression, obtained with proper linearization of the longitudinal phase space, limits the normalized emittance growth to values below the design goal of 1.5 μm, up to a compression factor of ~15, for a bunch charge of 500 pC.

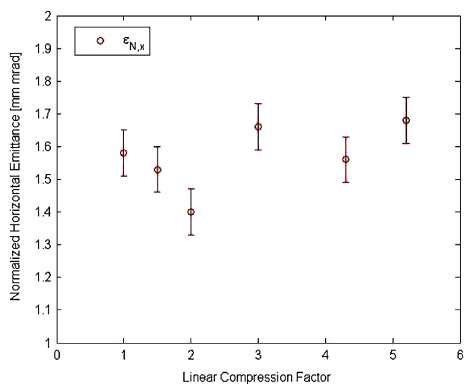

Figure 2: Horizontal normalized emitance of a 200 pC beam, measured out of BC1 as function of C. Published in [6].

ISBN 978-3-95450-126-7

GTW in Geometric Collimator

In linac-driven light sources, collimators are metallic blocks that prevent halo particles from hitting the vacuum chamber and creating electromagnetic showers that can destroy electronics and/or demagnetize permanent magnet blocks in undulators. The collimators are designed to restrict the vacuum chamber physical aperture without affecting the main beam. Usually, the collimator aperture is of the order of few millimeters. Depending on the bunch charge, the bunch length and the collimator geometry, a small aperture could generate significant transverse wake fields that impart a kick to the beam. This kick strength is correlated with the particle longitudinal coordinate. As a consequence, the collimator wake field can increase the projected emittance by head-tail lateral displacement.

A two-stage geometric collimation system is installed right downstream of BC1 [16]. We examined the single-pass effect of our 2 mm iris radius, longitudinally tapered collimator upon the ultra-relativistic, 500 pC, 2.4 rms long high brightness electron beam [17]. At least four other works [18–21] report direct measurements of kick factor of tapered collimators with the purpose of benchmarking analytical models of the wake field. The kick factor, which is related to the geometric transverse wake potential, allows the evaluation of the projected emittance growth through the beam matrix formalism:

$$\gamma\varepsilon_x = \gamma\sqrt{\varepsilon_{x,0}^2\left(1+\frac{\beta_x}{\varepsilon_{x,0}}\theta^2\right)}, \qquad (2)$$

$$\theta = \frac{hQ\kappa}{E}$$

where Q is the bunch charge, h is the bunch centroid distance from the collimator axis, κ is the rms kick factor in the plane of interest – the transverse rms kick averaged over the length of the beam – and E is the beam mean energy.

In the experiment, the electron beam was moved off center in the collimator, while looking at its position at one Beam Position Monitor (BPM) installed very close to the collimator itself. Figure 3 shows the polynomial fitting of the measured emittance as function of the beam offset in the collimator. The effective kick factor that characterizes the FERMI collimator was found to be κ_{fit} = 2.20 V/pC/mm, in agreement with the 3-D numerical evaluation of the wake potential for such a geometry (≤ 4 V/pC/mm) [22] and with the rms kick simulated for an almost identical geometry adopted at FLASH (2.04 V/pC/mm) [23]. FERMI routinely adopts 6 of similar collimators in dispersion-free as well in dispersive regions, with inner radius between 2 and 3 mm. Trajectory control within some tens of micron at close by BPMs turns out to be enough to avoid any $B_{4D,n}$ degradation.

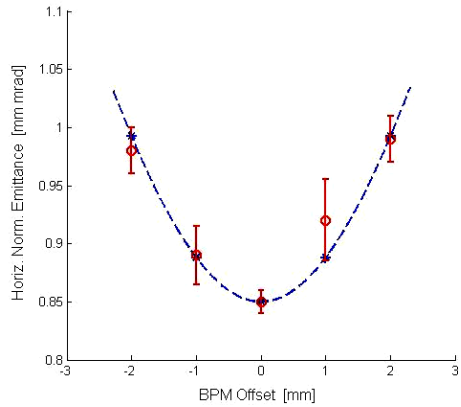

Figure 3: The horizontal normalized emittance vs. the BPM horizontal offset. The geometric collimator is set to 2 mm half-gap hole. The error bars show the maximum uncertainty of four consecutive emittance measurements. The quadratic term of the fit corresponds to a kick factor of κ_{fit} = 2.20 V/pC/mm. The dashed curve shows Eq. 2 evaluated for $\kappa = \kappa_{fit}$. Published in [17].

GTW in RF Linac

After leaving the BC1 area, the electron beam enters a 6 m long, high gradient, small iris accelerating structure. The single-bunch projected emittance dilution and the banana shape distortion [24] induced by short-range GTW in the FERMI linac [25] is particularly instructive because two different regimes of the instability can be detected in the same beam line. The passage from weak to strong instability, that is from small to large emittance degradation, is essentially due to the larger amplitude of the transverse wake function (more than one order of magnitude) in the high energy part of the line with respect to that at lower energy. That is turn related to the smaller average iris radius of ~5 mm at high energy, compared to ~9 mm at low energy. Figure 4, left plot shows the simulated projected emittance behavior when only one-to-one trajectory correction is implemented. Emittance suffers of some degradation up to the middle of the linac, and blows up as the beam enters the smaller iris structure, with consequent total disruption of the beam brightness. In the right plot, trajectory (emittance) bumps [26] are performed in the high energy part of the line to recover the initial emittance values, in both planes.

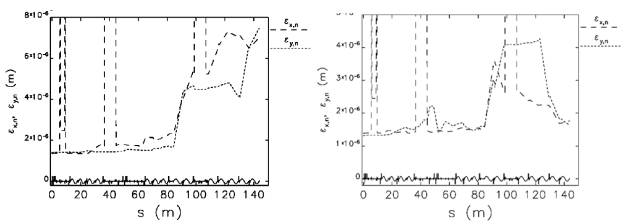

Figure 4: Normalized transverse emittances along the FERMI linac for 200 μm random rms linac misalignment, with only one-to-one trajectory steering (left) and with additional emittance bumps (right). Published in [25].

ISBN 978-3-95450-126-7

Trajectory bumps were systematically applied during commissioning, in the last region of the FERMI linac to minimize the projected emittance at the linac's end. Figure 5 shows the final emittance behaviour during the first semester of 2012, for different bunch charges and compression factors. BPM offsets were varied for each new machine working point in order to define a "golden" trajectory that allows net cancellation of the GTW effect at the linac's end. Curently, best performance ensures 1.5–2.0 μm normalized emittances, with < 0.3 μm emittance growth, in both planes, from BC1 to the linac's end, for a bunch charge of 500 pC and length of 1 ps full width.

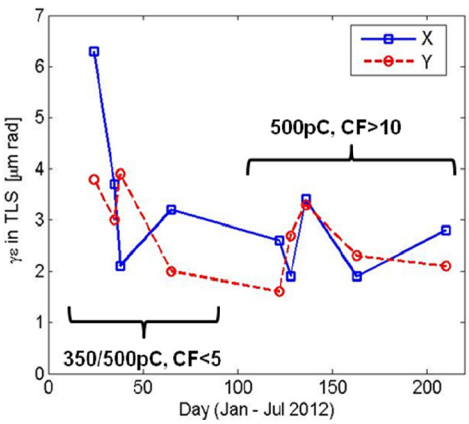

Figure 5: Projected normalized emittances at the linac's end during first semester of 2012.

CSR in the Spreader

The FERMI linac is connected to the undulator by the Spreader, a dog-leg made of two modified double bend achromats with many quadrupoles in between consecutive dipole magnets. Four identical dipole magnets bend the beam by 3 deg each. Emission of CSR as a contributing factor to emittance degradation is an important phenomenon in this region owing to the fact that the beam is fully compressed. A method to cancel this perturbation by imposing certain symmetric conditions on the electron transport system has been suggested in [27]. We expanded on this idea by quantitatively relating the beam Courant-Snyder parameters to the emittance growth, and by providing a general scheme of CSR suppression with asymmetric optics [28]. We recall in Figure 6 the experimental evidence of this cancellation of multiple CSR kicks: the transverse emittance of a 500pC, sub-ps, high brightness electron beam was preserved after the passage through the Spreader; conversely, emittance growth was observed when the optics balance was intentionally broken. We show the agreement between the theoretical model and the experimental results. This study holds the promise of compact dispersive lines with relatively large bending angles, hence with cost saving for future electron facilities.

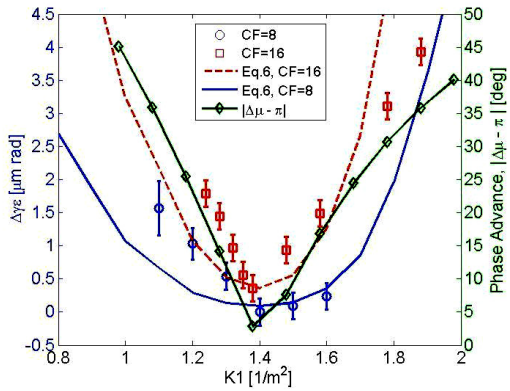

Figure 6: The horizontal normalized emittance growth at the end of the Spreader (markers with error bars) was measured as a function of the strength of a quadrupole placed in the middle of the Spreader. The squares (circles) are for C = 16 (8). The horizontal betatron phase advance between the achromats (diamonds) was computed with ELEGANT code [29] on the basis of the experimental machine settings; the absolute value of its distance from π is also shown. The dashed (solid) line is the analytical prediction for the emittance growth for C=16 (8). Published in [28].

4-D BRIGHTNESS OPTIMIZATION

It should be clear from these discussions that CSR and GTW, which have traditionally been treated separately in the archival literature, play a major role in the transverse emittance degradation. In this Section we formulate a limit on the final electron beam $B_{4D,n}$ imposed by the interplay of GTW in accelerating structures and CSR in magnetic compressors. We support the thesis presented in [30] according to which they are coupled by the variation of the bunch length along the beam line, and thus should be studied simultaneously. Experimental data validate this model, as shown in Figure 7.

More specifically, we aim to demonstrate that an optimum working point, namely one with the highest $B_{4D,n}$, can be found based on theoretical considerations. The physical reason for this claim is particularly evident in the simpler case of one-stage compression, and under the assumption that most of the GTW instability develops after the compressor. For any given charge, CSR induced emittance growth is inversely proportional to the bunch length at the end of the compressor. On the contrary, emittance degradation due to GTW instability is proportional to the compressed bunch length. Consequently, there should be an optimum bunch length after compression that minimizes the combined effect of GTW and CSR on the transverse emittance at the linac's end. For any desired final peak current, at most three parameters are necessary to achieve the optimum configuration, bunch charge, initial bunch length and compression factor. As a practical case study, Figure 8 shows that a $B_{4D,n}$ ~10^{16} A/m^2 can be reached with a 100 pC charge beam in the FERMI@Elettra accelerator with the existing machine configuration; this is a brightness approximately two orders of

ISBN 978-3-95450-126-7

magnitude higher than presently achieved with a charge of 500 pC.

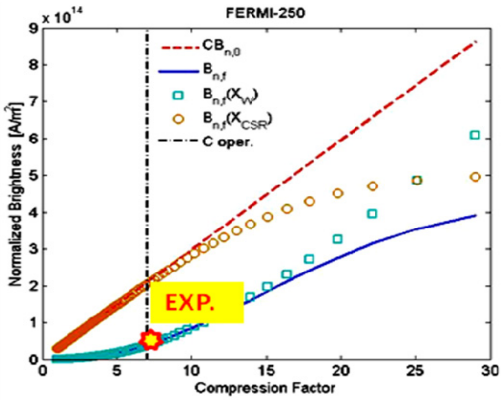

Figure 7: Theoretical final normalized brightness in FERMI as a function of the compression factor, for 250pC beam charge. The nominal (unperturbed) brightness is in dashed line, the effective (perturbed) brightness is in solid line, CSR (circles) and GTW dominated brightness (squares) is also shown. The dash-dot lines identify the operational compression factor. Published in [30].

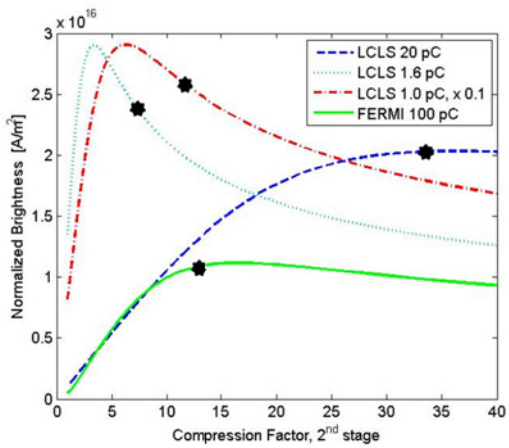

Figure 8: Final normalized brightness of low charge beams as a function of the compression factor in the second compressor of LCLS and FERMI. The star identifies the compression factor that is needed to a reach 1.5 kA final peak current. Published in [30].

CONCLUSIONS

Current FERMI operation takes advantage of systematic emittance studies carried out in 2012 and 2013 to maximize the final $B_{4D,n}$. The best performance for 500pC bunch charge delivered a projected normalized emittance of 1.5–2.0 μm in front of undulator. Individual contributions to the projected emittance growth are summarized in Figure 9. Slice emittance is approximately preserved at 1 μm level [2]. This best performance meets the FEL requirements and allows lasing within users' specifications. We acknowledge that, notwithstanding the validity of the model reported here, some empirical tuning is still needed to minimize the final emittance. This is not, however, critical for FEL operation. The model developed for the final $B_{4D,n}$ agrees with experimental data and promises further optimizations of the FERMI's working point.

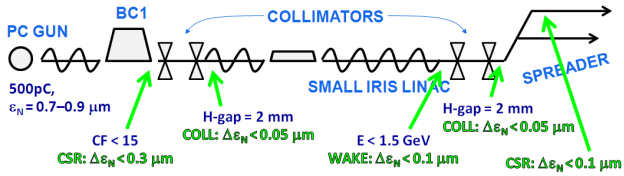

Figure 9: Projected emittance budget in the FERMI linac, current operation.

ACKNOWLEDGEMENT

Work supported in part by the Italian Ministry of University and Research under grants FIRB-RBAP045JF2 and FIRB-RBAP06AWK3.

REFERENCES

[1] C. J. Bocchetta et al., FERMI@Elettra FEL Conceptual Design Report, </http://www.elettra.trieste.it/FERMI> (2007).
[2] E. Allaria et al., Nat. Phot. 6, 699 (2012).
[3] H.P. Freund and P.G. O'Shea, Phys. Rev. Letters, 80, 3 (1998).
[4] S. Reiche, Nucl. Instr. Meth. Phys. Research A 445 (2000) 90–94.
[5] G. Geloni, V. Kocharayan and E. Saldin, DESY 11-081 (2011) arXiv:1105.3878v1.
[6] S. Di Mitri, E.M. Allaria, P. Craievich, W. Fawley, L. Giannessi, A. Lutman, G. Penco, S. Spampinati, and M. Trovo', Phys. Rev. ST Accel. Beams **15**, 020701 (2012).
[7] S. Di Mitri, M. Cornacchia, C. Scafuri and M. Sjöstrom, Phys. Rev. Special Topics Accel. Beams 15, 012802 (2012).
[8] G. Andonian et al., Phys. Rev. Letters 95, 054801 (2005).
[9] G.Penn et al., ST/F-TN-06/01 (2006).
[10] A.Lutman, et al., J. Phys. A: Math. Theor. 42 (2009).
[11] B. Jia et al., Phys. Rev. ST Accel. Beams 13, 060701 (2010).
[12] K. Flöttmann, T. Limberg, P. Piot, DESY-TESLA-FEL-2001-06 (2001)
[13] P. Emma, LCLS-TN-01-1 (2001).
[14] S. Di Mitri and M. Cornacchia, submitted to Nucl. Instr. Meth. Phys. Research A (2013).
[15] E.L. Saldin, E.A. Schneidmiler and M.V. Yurkov, Nucl. Instr. Meth. Phys. Res. A 398 (1997) 373 – 394.
[16] S. Di Mitri, Phys. Rev. ST Accel. and Beams **13**, 052801 (2010).
[17] S. Di Mitri, L. Fröhlich, E. Karantzoulis, Phys. Rev. ST Accel. and Beams **15**, 061001 (2012).
[18] N. K. Watson et al., in Proceedings of the 10th European Particle Accelerator Conference, Edinburgh, United Kingdom (2006), MOPLS066.
[19] I. Zagorodnov and K. Bane, in Proceedings of the 10th European Particle Accelerator Conference, Edinburgh, United Kingdom (2006), THPCH036.

ISBN 978-3-95450-126-7

[20] S. Molloy et al., in Proceedings of the 22nd Particle Accelerator Conference, Albuquerque, New Mexico (2007), FRPMS074.
[21] P. Tenenbaum, K.L.F. Bane, L. Eriksson, J. Irwin, R.K. Jobe, D. McCormick, C.K. Ng, T.O. Raubenheimer, M.C. Ross, G. Stupakov, D. Walz, D. Onoprienko, and I. Zagorodnov, Phys. Rev. ST Accel. and Beams **10**, 034401 (2007).
[22] S. Ferry, C. Bontoiu, P. Craievich, S. Di Mitri and E. Karantzoulis, in Proceedings of the 23rd Particle Accelerator Conference, Vancouver, Canada (2009), WE6RFP043.
[23] A. Tsakanian, M. Dohlus and I. Zagorodnov, Nucl. Instr. and Meth. in Phys. Research A **659** (2011) 9 – 13.
[24] A. Chao, et al., SLAC-PUB-2498, 1980.
[25] P. Craievich, S. Di Mitri and A. A. Zholents, Nucl. Instr. Phys. Res. A, 604 (2009) 457 – 465.
[26] P. Eliasson, D. Schulte, PRST-AB 11 (2008) 011002.
[27] D. Douglas, JLAB-TN-98-012 (1998).
[28] S. Di Mitri, M. Cornacchia and S. Spampinati, PRL 110, 014801 (2013).
[29] M. Borland, Advanced Photon Source LS-287 (2000).
[30] S. Di Mitri, Phys. Rev. ST Accel. Beams 16, 050701 (2013).

ISBN 978-3-95450-126-7